Static and fatigue failure analysis of adhesively bonded thick composite single lap joints

Tang, J. H.; Sridhar, I.; Srikanth, N.

2013

Tang, J. H., Sridhar, I., & Srikanth, N. (2013). Static and fatigue failure analysis of adhesively bonded thick composite single lap joints. Composites Science and Technology, 86, 18-25.

https://hdl.handle.net/10356/102341

https://doi.org/10.1016/j.compscitech.2013.06.018

Appeared in "Composites Science and Technology 86 (2013) 18–25", Elsevier Journal

Static and fatigue failure analysis of adhesively bonded thick composite single lap joints

J.H. Tang[a], I. Sridhar[a,b,*], N. Srikanth[b,]

[a]*School of Mechanical and Aerospace Engineering, Nanyang Technological University, 50 Nanyang Avenue, Singapore 639798*
[b]*Energy Research Institute @ NTU, 1 CleanTech Loop, Singapore 637141*

Abstract

Static and fatigue behavior of thick composite laminate single lap joints with thick adhesive bondline is experimentally and numerically investigated. Stress based analysis is used to understand the uniaxial tensile behavior of thick glass fiber reinforced epoxy laminates bonded with relatively thick epoxy adhesive. The effect of adhesive thickness on relatively thick adherend on the fatigue initiation life was modeled with generalized stress singularity approach. It was observed that the failure onset always occurred at adherend-adhesive interface. Subsequent crack propagation mostly resulted in interlaminar failure of adjacent first angle ply near to this interface. Both static and fatigue strength values decrease with increase of bondline thickness. Evaluation of generalized stress intensity factors of the corner geometry (square edge joint) provided a good correlation between predictions and experimental measurements.

Keywords: A. Adhesive joints, B. Fatigue, B. Interface, C. Finite element analysis

1. Introduction

Fiber reinforced composite materials possess high specific strength and stiffness, and are widely used in various engineering industries such as aerospace, automobile, marine, wind turbine and defense applications. Due to limited manufacturability of fiber reinforcement composites, complex shapes from these materials are mostly achieved either by using mechanical joining with rivets and bolts or adhesive bonding technique. Adhesively bonded composite joints are often favorable in consideration of reduction in stress concentration compared to bolted or riveted joints, and elimination of inherent fabrication damage induced by the fastener holes in bolted or riveted joints. Thick composite laminates are mostly employed for high rigidity and high load bearing applications in their

*Corresponding author.
Email address: msridhar@ntu.edu.sg (I. Sridhar)

principal direction. The compliant response resulting from the structural employment of adhesively bonded joints should be kept to minimum. This type of design constraint can be found in blade design of wind turbine where the excessive out-of-plane deflection of adhesively bonded spar under aerodynamic loads should be minimized to avoid collision with the tower. With respect to this design constraint, structural adhesives (mostly epoxy-based) are generally selected as a bonding material in thick composite laminates bonded joints. Brittle structural adhesive becomes advantageous as it exhibits high strength properties, in order to fully maximize the loading capacity of composite structural materials, and higher elastic modulus (compared with ductile adhesive), so that overall bonded structural responses could remain within specified design tolerance.

The importance of bondline thickness should not be overlooked. It was experimentally demonstrated that a thicker bondline would tend to reduce the strength of metallic as well as composite single lap joints [1–6], with the exception of joints bonded with elastometric adhesive [7]. Whereas, classical analytical stress based solutions of single lap joints [8, 9] predict increasing load bearing capacity with increasing bondline thickness. Adams and Peppiatt [10] suggested that ~~increased~~ chances of having porosity and microcrack in joints with thicker bondline ~~as a reason for strength reduction in single lap joint~~. By considering plastic behavior of adhesive, Crocombe [1] showed that the global failure (yielding) of adhesive can lead to lowering of load bearing capacity as bondline thickness increases. With thicker bondline, the rate at which the yielding zone develops is faster, and hence an early failure. Gleich et al [11] have interpreted bondline effect, especially for high-strength and brittle adhesive, by acknowledging that both the stress concentration and singularity at the adhesive-adherend interface become more intense as bondline thickness increases. Among the other variables, optimum thickness can be a specific characteristic of the bondline. A few researchers [3, 11] suggest that an optimum bondline thickness should ideally be kept between 0.1 mm–0.5 mm. Van Tooren et al [12] verified that this optimum thickness could be well correlated with the variation of critical generalized stress intensity factor evaluated at critical (geometry) corner of a single lap

joint. Theoretically, having a range of optimum bondline thickness is not well understood: Kinloch and Shaw [13] suggested that maximum fracture energy develops due to distortion of plastic zone size caused by constraining effect of more rigid adherend, while Gleich et al [14] hypothesized that, for very thin bondline thickness, interaction between two close stress singularities starts to occur should the thickness falls below an optimum range.

The relative thickness of adherend to bondline is of another practical concern. For comparison, it is noted that the experiment studies undertaken by van Tooren et al [12] had focused on relative thin (~2 mm) adherends compared to adhesive bondline thickness (0.1 mm to 6 mm). As for applications involving thick (~8 mm) composite laminates as adherends, the laminates' fabrication processes do not have the luxury of consistently maintaining a uniform adherend thickness throughout the bonded area. This *variability* of bondline thickness has been identified to be major concern because of inclination of thinner bonded area to attract more load and to cause stress concentration in adjacent adherends. It is noted that a ± 0.254 mm variation in a nominally 0.254 mm bondline thickness is far more detrimental than same variation in a nominally 2.5 mm bondline thickness [15]. And thicker the laminate is, likelihood of occurrences of ply wrinkling, increased porosity, renders the thickness variability inevitable in practice. Likewise, the warping tendency of the finished composite panels caused by processing tool and manufacturing cycle presents similar challenge when intended panels are to constitute the final structure consisted of adhesively bonded joint. Shrinkage gradient during the laminates curing further changes the dimensions of it, especially in thicker composite panels. Hence, uniformly maintaining a bondline thickness to 0.1–0.5 mm range may not be an ideal as well as practical bonding strategy.

In non-structural members, like upper and lower wing skins of a wind turbine blade structure, the gap formed by both wing skins at leading edge is adhesively filled, and thus forms a thick adhesively bonded joint. These non-structural adherends will be subjected to fatigue load resulting from the fluctuation of aerodynamic load. Most of the literature on

fatigue life of joints were based on the framework of strain energy release rate for fatigue crack propagation, which usually leads to an overestimate of fatigue life, ignoring the life needed for crack initiation. On the influence of various parameters such as joint geometries, failure modes, adhesive properties on the static as well as fatigue failure of adhesive composite joints, de Goeij et al [16] made a comprehensive compilation of experimental and analytical methods that exist in literature. For the single lap joint, very few studies [17–20] can be found to have attempted to include the bondline thickness effect in fatigue analysis. Among these studies, only concrete evidence of decreasing fatigue strength as bondline thickness increases was reported by Harris and Fay [17], and Jen and Ko [20]. In the studies of Jen and Ko [20], the fatigue strength of aluminium single lap joints with thickness ranged from 0.5 mm to 1.5 mm was correlated using simulated interfacial stress parameters on account of interfacial crack initiation between adhesive and aluminium. It was also reported that interfacial peel stress is a more dominant parameter responsible for the fatigue crack initiation. A generalized stress intensity factor approach was applied in fatigue crack initiation of composite single lap joints by Quaresimin and Ricotta [21, 22], and Meneghetti et al [23]. When coupled with the evaluation of strain energy release rate for fatigue crack propagation, this approach appeared promising for analyzing the damage evolution at adhesive-adherend interface. Still, it is yet to be testified in the case of relatively thick adhesively bonded single lap joints.

Furthermore, it becomes compelling to consider a relative thick bondline whenever thick adherends are used in composite single lap joints, in view of the thickness variability of thick adherend. It is the aim of this paper to provide a validation pertinent to fatigue crack or failure initiation in thick bondline thickness, using the approach of generalized stress intensity factors. This paper also investigates the peel and shear stresses of thick laminate single lap joints with thick bondline thickness under uniaxial tensile loading, and shows how it is inadequate to merely approach the failure criterion by stress based analysis. The paper further demonstrates how, in the context of thick adherend with thick bondline, the methodology using the approach of generalized stress intensity factors can

be successfully applied in static as well as fatigue failure initiation prediction.

2. Failure initiation criterion

The generalized stress intensity factor approach has been proposed and adopted to quantify the failure initiation criterion in bonded joints by several authors [14, 24–28]. The aim of this paper is to further validate the suitability of this approach in the context of thick laminate single lap joints. Not only this approach had been illustrated to correlate better with the variation of bondline thickness, as illustrated by van Tooren et al [12], in term of static failure initiation of single lap joint, but also can be used to establish a fatigue crack initiation criterion for a particular geometry corner, as presented by Quaresimin and Ricotta [21]. As the location of failure onset corresponds to location of sharp corner (which is point of high stress concentration as well as stress singularity) in the bonded joints, it makes no ambiguity that generalized stress intensity factor evaluated at singularity can be used as failure initiation criterion for the bonded joint. With lower stress level and reduced plasticity encountered in fatigue loading, the applicability of this approach is expected to improve [27]. It is to be noted that fatigue life of a composite joint can be divided into two phases, one for the crack initiation and another one for its propagation. The Paris law along with strain energy release rate over the overlap length can be used to predict the crack propagation life, which is commonly applied to estimate the fatigue life of adhesively bonded joints. Despite the possibility that substantial fatigue life may be spent on crack or failure initiation phase, very few researchers had tried to investigate the crack initiation life. A fatigue life modeling incorporating both crack initiation and propagation phase was only recently proposed by Quaresimin and Ricotta [21], by means of evaluation of the generalized stress intensity factor and strain energy release rate, respectively for each phase.

At the bi-material corner of bonded single lap joint, the singular stresses in the near vicinity of the interface corner are generally controlled by two singularity terms given by

[27–29]:

$$\sigma_{ij}(r,\theta) = H_1 r^{-\lambda_1} \cdot f_{ij}^{(1)}(\theta) + H_2 r^{-\lambda_2} \cdot f_{ij}^{(2)}(\theta) \quad (1)$$

The generalized stress intensity factors H depend on boundary conditions (joint geometry and applied load) while the eigenvalues λ (or singularity orders) are related to the bi-material wedge angle and elastic properties of adherend and adhesive. Though the eigenvalues λ may be analytically evaluated, the generalized stress intensity factors would be conveniently obtained through finite element analysis, as complex geometry and various possible far field boundary conditions of a bonded joint suggest that it may be ineffectual to attempt an analytical solution.

3. Joint preparation and testing parameters

The single lap joints (SLJs) were made of glass fiber reinforced epoxy matrix composite laminates as adherends of equal nominal thickness of 8 mm with an overlap length of 40 mm. The laminates were made from stitch bonded left-hand and right-hand triaxial (0° warp, ±45° bias) reinforcement fabrics with the lay-up of $(\pm 45/0)_{3s}$, by employing resin transfer molding process. To investigate the effect of adhesive thickness on static and fatigue performance, two different bondline thicknesses, i.e. 2.5 mm or 5.5 mm, of SLJs were selected. Due to manufacturing problems the GFRP laminates thickness varies in between 8.12 mm to 8.35 mm. The laminates were cut into adherend size, as shown in Figure 1, prior to bonding with epoxy resin. Two-part (resin-hardener) epoxy adhesive, trade name Spabond 340 (produced by Gurit) was used as bonding material. To achieve the required nominal adhesive thickness, the laminates were held by wooden fixture before allowing for the curing of adhesive. Aluminium end tabs were mounted on both loading ends of the adherend with equal width as the adherend. Both aluminium end tabs and adherend surfaces were roughened with the use of emery paper and cleaned with acetone. The same Spabond adhesive used to bond the adherends was used to bond the aluminium end tabs. As per manufacturer's (Spabond) standard, the joints were produced by curing the bonded laminates at room temperature for 24 hours and post-curing at 50 °C

for 16 hours.

Both the uniaxial static tensile and fatigue tests were conducted on a servo-hydraulic MTS 810 Material Testing System with 100 kN load cell. The static tests were carried out under displacement control at a crosshead speed of 0.6 mm/min. Strain values were measured at four distinct locations on the adherends, at selected SLJs, to validate the response from finite element analysis. Exact locations where these strain gauges (denoted by SG-1, SG-2, SG-3 and SG-4) of 3 mm gauge length and 350 Ω resistance were mounted are depicted in Figure 1. ~~The~~ fatigue tests were conducted under load control, with sinusoidal waveform at a frequency of 5 Hz. The load ratio (maximum tensile load/minimum tensile load), R was set to 0.1 in all the tests. All the tests were conducted at room temperature condition of 23 °C and 55±5 % relative humidity. Fatigue tests were stopped whenever the total number of cycles reached 10^6, if there was no total separation between both adherends. Note that the geometry configurations of the SLJs adopted in this paper has no association with geometry of ASTM D3165 and D5656.

4. Modeling approach

Commercial finite element package ABAQUS/Standard was used to simulate the mechanical response of the composite single lap joints under quasi-static loading. Two-dimensional (2D) finite element modeling was developed using plane strain quadratic element CPE8, by assuming all materials to be elastic with geometric linearity. A uniaxial tensile test on bulk Spabond adhesive revealed that the Young's modulus to be 1.98 GPa with Poisson's ratio of 0.35 so that the bondline was modeled as isotropic material with these properties. The GFRP composite adherends were modeled as bulk orthotropic material and its material properties are: in-plane Young's modulus E_{11}, 36.80 GPa; in-plane Young's modulus E_{22}, 15.38 GPa; through-thickness Young's modulus E_{33}, 3.30 GPa; Poisson's ratio ν_{12}, ν_{13} and ν_{23} are respectively 0.40, 0.30 and 0.32; in-plane shear modulus G_{12}, 3.26 GPa; through-thickness shear modulus G_{13}, 1.02 GPa; and through-thickness shear modulus G_{23}, 1.89 GPa. Note that 1-3 laminate plane corresponds to 1-2

plane of the 2D finite element modeling.

For the evaluation of stress distribution along the overlap length, mesh refinement was symmetrically performed until stress profile at the mid-plane of bondline layer has converged, i.e. when the smallest element size near the concentration region reached 0.25 mm. Since detailed finite element and experimental studies revealed the brittle behavior of adhesive is valid up to first failure initiation, a linear elastic constitutive model for the adhesive is deemed sufficient. For the sake of totality of overall mechanical response, the aluminium tab was modeled as an elastic material with Young's modulus of 70 GPa and Poisson's ratio of 0.33. The applied traction at the gripping surfaces of aluminium tab amounts to an equivalent load of 200 N/mm on the SLJ and the other simulated boundary conditions are given in Figure 1.

Only for the evaluation of generalized stress intensity factors at the geometrical corner, i.e. at the square edge corner of adhesive fillet, extreme mesh refinement was achieved by using a bias ratio of 100 with 50 elements, within radial distance of 0.07 mm from the apex. Also at the apex, 12 triangle elements CPE6 were created. The smallest element size of this singularity zone modeling is of the order of 10^{-5} mm and the resulting meshing scheme around the square edge corner is shown in Figure 1. In the current study, the generalized stress intensity factors evaluated at the adherend-adhesive interface ($\theta = 0$) are of interest. Considering this special case, equation (1) can be reduced to

$$\sigma_{ij}(r) = H_{ij}^{(1)} r^{-\lambda_1} + H_{ij}^{(2)} r^{-\lambda_2} \tag{2}$$

where H_{22} and H_{12} shall be respectively referred to peel stress intensity factor and shear stress intensity factor in the later part of this paper. The eigenvalues for an isotropic-orthotropic corner may be first evaluated using procedures outlined by Barroso et al [30], making use of the concept of transfer matrix. Through finite element analysis, the values of generalized stress intensity factors can be conveniently calculated by curve-fitting technique (though it may also be otherwise evaluated using closed path integral method,

as presented by several authors [31–33]).

5. Results and discussion

5.1. Quasi-static loading

Figure 2 shows the comparison of effect of the bondline thickness has on the load-displacement curves of SLJs (6 specimens tested for each thickness). Until the initial failure load is reached, the load-displacement response is quite linear and then there is a sudden drop in load. In most SLJs, a second gradual increase in the load are found before failing catastrophically. The compliance of SLJs with 5.5 mm thick bondline is about 1.3 times that of the 2.5 mm due to increased apparent shear deformation induced in thicker bondline. The longitudinal strains measured using the strain gauges at location shown in Figure 1 are in good agreement with the finite element simulations, as illustrated in Figure 2. It can be construed that with higher bondline thickness, higher bending moments prevail at adherend arms due to greater eccentricity of axial loading.

Table 1 summarizes the average values of critical load at which the first failure initiation occurred at the square edge corner of adhesive bondline. Following the initiation failure at interface, which also come along with detection of "cracking" sound, visible initial crack (~5 mm) length, by means of naked eye observation, can be noticed along the adhesive-adherend interface. The crack propagation was very unstable and characterized by the presence of the crack that suddenly jumped from 0 to ~5 mm, propagating at the adhesive-adherend interface. As the quasi-static loading continued to build up after initial load drop caused by initiation, a second failure mode took place catastrophically, whereby ripping of first $\pm 45^\circ$ plies as well as delamination between principal and this $\pm 45^\circ$ plies occurred, resulted in adherend total separation. This final failure mode, namely mixed interfacial-interlaminar failure mode, is illustrated in Figure 3(a), where fiber pull-out of first $\pm 45^\circ$ plies is indicated by whitening zone on the overlap region. As shown in Figure 3(b), the other possible final failure mode is pure interfacial, following the interfacial crack initiation. Its occurrences also took place catastrophically and it happened in 17 %

of the SLJs (refer to Table 1). In instances whereby adherend total separation did not occur despite occurrence of interlaminar (delamination) failure between principal and $\pm 45^\circ$ plies, due to default machine protective set-up, ripping or pull-out of the first $\pm 45^\circ$ plies was not observed, as depicted by fiber/ply bridging shown in Figure 3(c).

5.1.1. Evaluation of stress distributions

Following the failure loads presented in Table 1, the behavior of decreasing strength of the SLJs with increasing bondline thickness could be explained by undertaking a stress based analysis. But the stress based analysis only produces fruitful results should one looks at the failure stresses of interface, as this physically correlates to observations manifested in experiment. As already emphasized in the investigations by Gleich et al [11], quite a substantial literature had illustrated the significant role of interface peel and shear stresses in determining the effect of bondline thickness. In the case of thick bondline, this paper further demonstrates how these interface stresses prevail despite the higher rigidity response of thick composite laminate adherend.

Figure 4 gives an overview of peel stress σ_{22} and shear stress σ_{12} computed by finite element analysis at two distinct overlap plane, i.e. at the exact interface of adhesive (denoted by $y/t_a = 0$) and the mid-plane of the bondline (denoted by $y/t_a = 0.5$). Here, the discrepancies of stresses at these two planes are apparent: asymmetric stress distributions are obtained at interface, with singularity stress field condition toward the square edge corner (overlap distance = 0); whereas symmetric stress distributions are obtained at the mid-plane, with decreasing behavior of peak stresses as bondline thickness decreases. Note that whether a singularity zone modeling is present or not, the asymmetric stress distributions at $y/t_a = 0$ are not affected. Additionally, the classical peel and shear stresses solutions derived from the work of Goland and Reissner theory [9] are also presented in Figure 4. Although the Goland and Reissner classical theory assumes a very large adherend's free arm over the overlap length with contant peel and shear stresses across the adhesive thickness, the solutions appear to give a satisfactory comparison with the stresses obtained at the mid-plane of bondline. The improvements made by various

researchers [34–36] in addressing the variation of stresses across the thickness direction meet its diminishing benefits, when rather thick bondline is considered. Also, the stress singularity exhibited by the interface corner would be meaningless when applying maximum stress data to engineering design of the bonded joints. An alternative strategy to deal with the stress singularity at the interface corner is what the approach of generalized stress intensity factors can offer.

5.1.2. Evaluation of generalized stress intensity factors

The eigenvalues for the bi-material corner adopted in current study were calculated using analysis presented by Barroso et al [30]. The possible effect of having a spew fillet on the eigenvalues is presented in Figure 5. Two real eigenvalues are obtained when the fillet angle reaches 89° and converted to two complex eigenvalues when the fillet angle reaches 156°. In the case of square edge corner (90° fillet angle), the eigenvalues are $\lambda_1 = 0.3579$ and $\lambda_2 = 0.0032$, and their corresponding generalized stress intensity factors obtained by means of curve fitting to the stress field close to the singularity are tabulated in Table 2. As $\lambda_2 \simeq 0$, there is a possibility of omitting the second singularity term, and the corresponding generalized stress intensity factor is also given. $H_{ij}^{(1)}$ terms given by this approximation, however, suffer a slight decrease in goodness of fit.

As the failure at interface is peel stress dominated, $H_{22}^{(1)}$ has been chosen as failure initiation criterion. In the present analysis, the failure at the interface corner is assumed to initiate when the chosen $H_{22}^{(1)}$ is greater than a critical generalized stress intensity factor H_{cr}. To give a more conservative analysis, values of $H_{22}^{(1)}$ without approximation are adopted. On the basis of two different bondline thicknesses investigated in the experiment, the critical generalized stress intensity factor H_{cr} for each thickness was tabulated in Table 1. Each calculation was obtained by multiplying the critical tensile load P_{cr} (also first initiation load) with the rate of change of generalized stress intensity factor with respect to applied tensile load $\mathrm{d}H_{22}^{(1)}/\mathrm{d}P_{\mathrm{FEM}}$ simulated from the finite element analysis. It can be noticed that, using H_{cr} as failure initiation criterion, failure loads correlate very well with the variation in both thicknesses. In a separate analysis, when the bondline thickness is

below 0.2 mm, the two singularity terms, as given in equation (2), with the eigenvalues of $\lambda_1 = 0.3579$ and $\lambda_2 = 0.0032$, no longer accurately captured the singularity stress field behavior. This suggests that interaction of singularities from both interfaces (90° and 180° wedge angle made by adherend) could start to occur, consistent with hypothesis given by Gleich et al [14].

5.2. Fatigue loading

The fatigue data are first presented using the classical load-life approach for both bondline thicknesses, i.e. 2.5 mm and 5.5 mm, followed by transformation of load-life data into $H_{22}^{(1)}$-fatigue-failure-initiation-life data by performing analysis of generalized stress intensity factors. Figure 6(a) summarizes the maximum nominal tensile load versus cycles to total failure response for the SLJs with both bondline thicknesses. It can be noticed that the SLJs with 5.5 mm bondline thickness exhibit lower fatigue strength, as in the quasi-static results. Fracture surface of typical fatigue failure mode of the SLJs is similar to ones portrated in Figure 3. In all of the joints, the failure of the joints *always* nucleated at one of the interface corners between the adhesive and adherends.

And in 80 % of the joints, this nucleation path continued to propagate along this interface, until at some propagation distance from the nucleation side, interlaminar (delamination) failure occurred between principal and first ±45° plies. Up to this point, the ripping or pull-out of the ±45° plies had not yet occurred, as characterized by fiber/ply bridging shown in Figure 3(c). This interlaminar failure created a second nucleation side for crack propagation. The crack propagation continued at both (adhesive-adherend and principal/±45° plies) interfaces before final failure by means of fast propagation, resulted in ripping or pull-out of the ±45° plies and adherend total separation, as illustrated by Figure 3(a). A simplified sequence of the damage mechanism is as such: interfacial nucleation at adhesive-adherend interface, then interfacial propagation, followed by interlaminar nucleation at principal/±45° plies, then both interfacial and interlaminar propagation and finally ripping of ±45° plies. As the failure in ±45° plies occurred last, the damage sequence is quite different from those reported by several researchers [23, 37–39]. For

damage to propagate as delamination between interface of principal and $\pm 45^{\circ}$ plies, these researchers observed a prior intraply failure in $\pm 45^{\circ}$ plies, and hence a continuation of a single propagation path. In view of the complex damage mechanism involved due to evolution of two propagation paths, the fatigue crack propagation phase using strain energy release rates was not analyzed in this paper.

Whereas in 20 % of the joints, the propagation continued to remain at initial nucleation (adhesive-adherend) interface, as illustrated in Figure 3(b). The cycles to failure initiation, cycles to total failure and final failure mode leading to adherends separation are given in Tables 3(a) and 3(b). From these tables, it can be noticed that there is no direct correlation between number of cycles to total failure with total failure mode so that there is not enough evidence to suggest a better fatigue life by promoting an interlaminar propagation phase.

5.2.1. Evaluation of the generalized stress intensity factors

Taking maximum nominal load range and bondline thickness into account, the load-life data are transformed into generalized stress intensity factor range ΔH versus number of cycles to fatigue crack initiation data ($\Delta H \equiv H_{\max} - H_{\min}$, where H is taken from $H_{22}^{(1)}$). The data are plotted in a log-log scale, as shown in Figure 6(b). For the material system considered in the current study, perhaps it is to be noticed that once $\Delta H < 0.3 H_{\mathrm{cr}}$, substantial increment in fatigue initiation life could be obtained. In this paper, the fatigue initiation cycles is defined as 5 % change in the initial maximum compliance (actuator displacement measured by the MTS inbuilt transducer divided by tension load measured by the load cell) of the SLJs' response. Visual inspection on selected SLJs showed that the crack initiation length is always less than 1 mm whenever 5 % compliance change occurred. This approach is different from detectable crack length of 0.3 mm using optical microscopy employed by Quaresimin and Ricotta [21]. It is worthy to note that SLJs with high nominal maximum load always failed catastrophically with negligible difference between initiation and propagation life, as tabulated in Tables 3(a) and 3(b). By assuming a power-law function between ΔH and cycles to fatigue initiation, the goodness of fit, R-square adjusted, is found to be 0.92. This justifies the feasibility of generalized stress

intensity factors approach in term of characterizing the fatigue life into single scatter band, irrespective of differences in geometrical parameters. This approach is also attractive in a sense that the fatigue initiation point always takes place at the square edge of the adhesive fillet, an observation similar to quasi-static case.

6. Conclusions

Quasi-static and fatigue behavior of single lap joints with thick adherends are investigated. The analysis focuses on the approach of generalized stress intensity factors in predicting the crack or fatigue initiation behavior of square edge corner at the critical adherend-adhesive interface of the single lap joints, with the aim of providing a validation of the approach by varying the bondline thickness.

For the geometrical parameters considered in this experiment, the failure was observed to be always initiated at the interface of the thick bondline, which renders the classical peel and shear stress analysis inaccurate in predicting the failure. Experimental results showed that quasi-static strength increases with decreasing bondline thickness, contrary to classical peel and shear stress analysis at the mid-plane of the thick bondline. The peel and shear stress evaluation at the interface appears to be more convincing in explaining the experimental observation but the singularity feature of both stresses suggests it could be conveniently quantified by the approach of generalized stress intensity factors. And the approach turns out to be excellent in capturing the effect of bondline thickness on the failure strength, in accordance with results presented by van Tooren et al [12]. The approach is further extended to provide a feasible prediction model for the fatigue failure initiation of single lap joints with thick bondline. The approach congregates the fatigue data given by the two bondline thicknesses in single scatter band, which provides a more unified analysis from physical standpoint. In applications where variability of a thicker adherend favors the exercise of thick bondline, the approach presented in this paper should prove useful in predicting the quasi-static failure and fatigue life responses.

For practical application, it is suggested that the fatigue life could be further improved

by eliminating the interface failure, possibly by making the interface much stronger by chemical/physical treatment of thick composite laminate prior to bonding with adhesive. Additionally, presence of spew fillets should help to reduce both the critical stress concentration and relative generalized stress intensity factors.

Acknowledgment

J.H. Tang thanks Nanyang Technological University for the financial support in the form of a Research Studentship. I. Sridhar and N. Srikanth thank Energy Research Institute @NTU (ERI@N) for material support.

[1] Crocombe AD. Global yielding as a failure criterion for bonded joints. Int J Adhes Adhes 1989;9:145–53.

[2] Tomblin J, Harter P, Seneviratne W, Yang C. Characterization of bondline thickness effects in adhesive joints. J Compos Tech Res 2002;24:332–44.

[3] da Silva LFM, Rodrigues TNSS, Figueiredo MAV, de Moura MFSF, Chousal JAG. Effect of adhesive type and thickness on the lap shear strength. J Adhes 2006; 82:1091–115.

[4] Kim KS, Yoo JS, Yi YM, Kim CG. Failure mode and strength of uni-directional composite single lap bonded joints with different bonding methods. Compos Struct 2006;72:477 – 485.

[5] Kahraman R, Sunar M, Yilbas B. Influence of adhesive thickness and filler content on the mechanical performance of aluminum single-lap joints bonded with aluminum powder filled epoxy adhesive. J Mater Process Technol 2008;205:183–9.

[6] Castagnetti D, Spaggiari A, Dragoni E. Effect of bondline thickness on the static strength of structural adhesives under nearly-homogeneous shear stresses. J Adhes 2011;87:780–803.

[7] Banea MD, da Silva LFM. Static and fatigue behaviour of room temperature vulcanising silicone adhesives for high temperature aerospace applications. Materialwiss Werkstofftech 2010;41:325–35.

[8] Volkersen O. Die nietkraftverteilung in zugbeanspruchten nietverbindungen mit konstanten laschenguerschnitten. Luftfahrtforsch 1938;15:41–7.

[9] Goland M, Reissner E. The stresses in cemented joints. J Appl Mech 1944;11:A17–27.

[10] Adams RD, Peppiatt NA. Stress analysis of adhesive-bonded lap joints. J Strain Anal 1974;9:185–96.

[11] Gleich DM, Van Tooren MJL, Beukers A. Analysis and evaluation of bondline thickness effects on failure load in adhesively bonded structures. J Adhes Sci Technol 2001;15:1091–101.

[12] van Tooren MJL, Gleich DM, Beukers A. Experimental verification of a stress singularity model to predict the effect of bondline thickness on joint strength. J Adhes Sci Technol 2004;18:395–412.

[13] Kinloch AJ, Shaw SJ. The fracture resistance of a toughened epoxy adhesive. J Adhes 1981;12:59–77.

[14] Gleich DM, van Tooren MJL, Beukers A. A stress singularity approach to failure initiation in a bonded joint with varying bondline thickness. J Adhes Sci Technol 2001;15:1247–59.

[15] Hart-Smith LJ. Adhesive bonding of composite structures - Progress to date and some remaining challenges. J Compos Tech Res 2002;24:133–51.

[16] de Goeij WC, van Tooren MJL, Beukers A. Composite adhesive joints under cyclic loading. Mater Des 1999;20:213–21.

[17] Harris JA, Fay PA. Fatigue life evaluation of structural adhesives for automotive applications. Int J Adhes Adhes 1992;12:9–18.

[18] Krenk S, Jonsson J, Hansen LP. Fatigue analysis and testing of adhesive joints. Eng Fract Mech 1996;53:859–72.

[19] Mazumdar SK, Mallick PK. Static and fatigue behavior of adhesive joints in SMC-SMC composites. Polym Compos 1998;19:139–46.

[20] Jen YM, Ko CW. Evaluation of fatigue life of adhesively bonded aluminum single-lap joints using interfacial parameters. Int J Fatigue 2010;32:330–40.

[21] Quaresimin M, Ricotta M. Life prediction of bonded joints in composite materials. Int J Fatigue 2006;28:1166–76.

[22] Quaresimin M, Ricotta M. Fatigue behaviour and damage evolution of single lap bonded joints in composite material. Compos Sci Technol 2006;66:176–87.

[23] Meneghetti G, Quaresimin M, Ricotta M. Influence of the interface ply orientation on the fatigue behaviour of bonded joints in composite materials. Int J Fatigue 2010; 32:82–93.

[24] Gradin PA. A fracture criterion for edge-bonded bimaterial bodies. J Compos Mater 1982;16:448–56.

[25] Groth HL. A method to predict fracture in an adhesively bonded joint. Int J Adhes Adhes 1985;5:19–22.

[26] Groth HL. Stress singularities and fracture at interface corners in bonded joints. Int J Adhes Adhes 1988;8:107–13.

[27] Lefebvre DR, Dillard DA. Stress singularity approach for the prediction of fatigue crack initiation in adhesive bonds. Part 1: Theory. J Adhes 1999;70:119–38.

[28] Quaresimin M, Ricotta M. Stress intensity factors and strain energy release rates in single lap bonded joints in composite materials. Compos Sci Technol 2006;66:647–56.

[29] Lazzarin P, Quaresimin M, Ferro P. A two-term stress function approach to evaluate stress distributions in bonded joints of different geometries. J Strain Anal Eng Des 2002;37:385–98.

[30] Barroso A, Mantic V, Paris F. Singularity analysis of anisotropic multimaterial corners. Int J Fract 2003;119:1–23.

[31] Sinclair GB, Okajima M, Griffin JH. Path independent integrals for computing stress intensity factors at sharp notches in elastic plates. Int J Numer Methods Eng 1984; 20:999–1008.

[32] Carpenter WC, Byers C. A path independent integral for computing stress intensities for v-notched cracks in a bi-material. Int J Fract 1987;35:245–68.

[33] Akisanya A. On the singular stress field near the edge of bonded joints. J Strain Anal Eng Des 1997;32:301–11.

[34] Allman DJ. A theory for elastic stresses in adhesive bonded lap joints. Q J Mech Appl Math 1977;30:415–36.

[35] Ojalvo IU, Eidinoff HL. Bond thickness effects upon stresses in single-lap adhesive joints. AIAA J 1978;16:204–11.

[36] Chen D, Cheng S. Analysis of adhesive-bonded single-lap joints. J Appl Mech, Trans ASME 1983;50:109–15.

[37] Meneghetti G, Quaresimin M, Ricotta M. Damage mechanisms in composite bonded joints under fatigue loading. Composites Part B 2012;43:210–20.

[38] Renton WJ, Vinson JR. Fatigue behavior of bonded joints in composite material structures. J Aircr 1975;12:442–447.

[39] Johnson WS, Mall S. Influence of interface ply orientation on fatigue damage of adhesively bonded composite joints. J Compos Tech Res 1986;8:3–7.

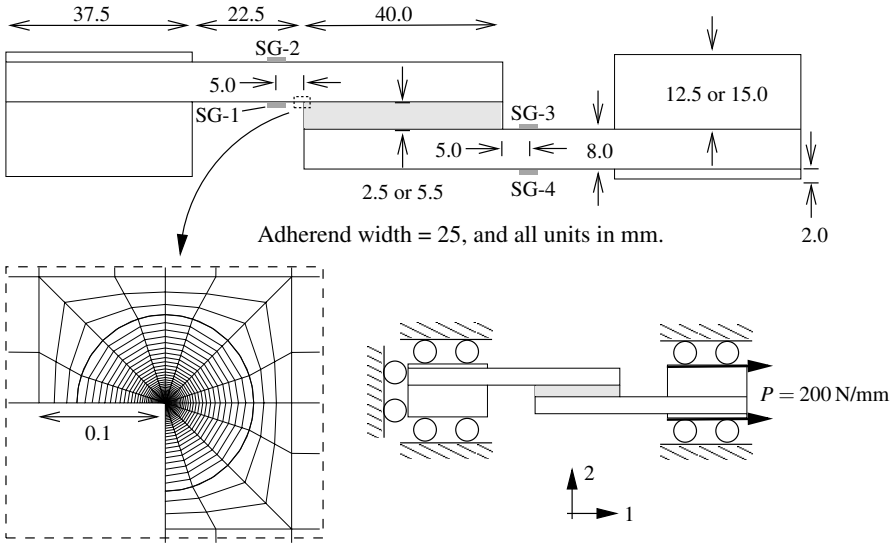

Figure 1: The single lap joint geometry adopted and the meshing scheme around critical singularity corner. SG stands for strain gauge.

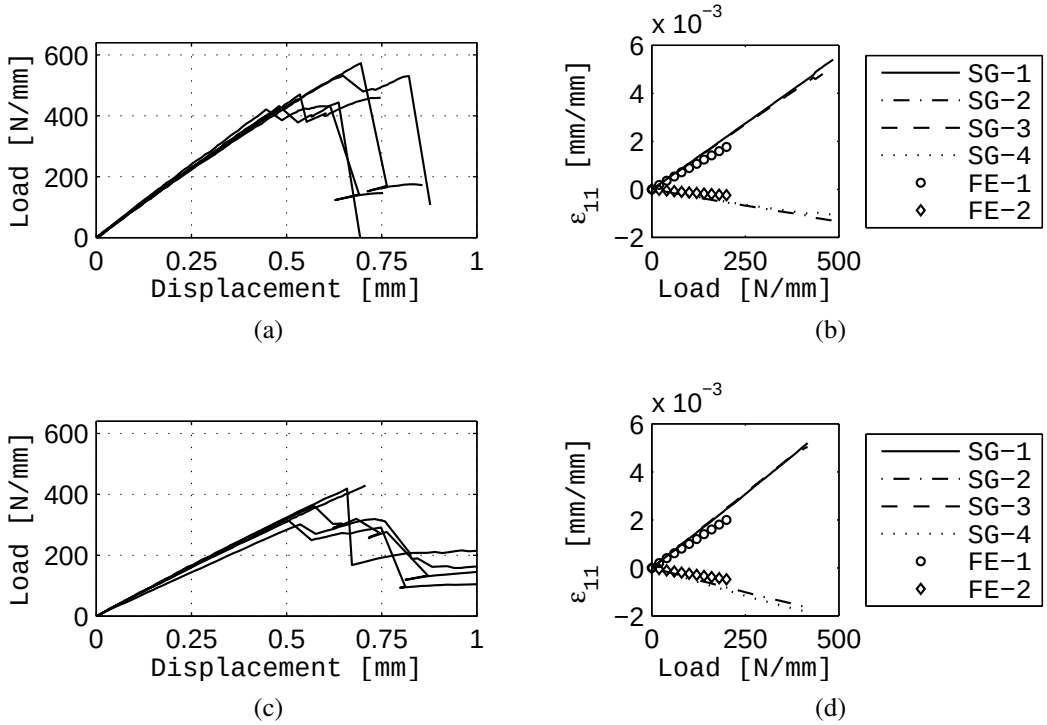

Figure 2: Measured load-displacement curves for tested SLJs and comparison between longitudinal strain ε_{11} measured from strain gauge (SG) and finite element (FE) simulation with adhesive thickness of 2.5 mm [(a) and (b)] and that of 5.5 mm [(c) and (d)].

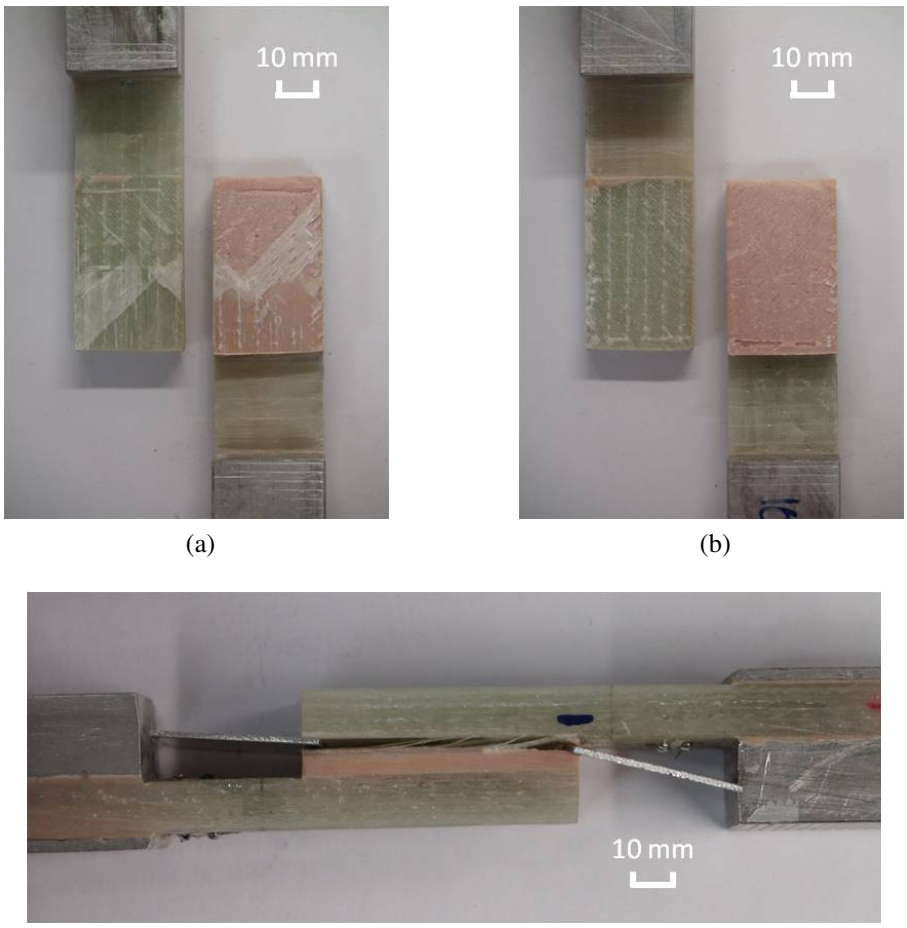

(a) (b)

(c)

Figure 3: Failure surfaces from: (a) mixed failure path (b) pure interfacial failure path (c) mixed failure with fiber/ply bridging, and no adherend separation.

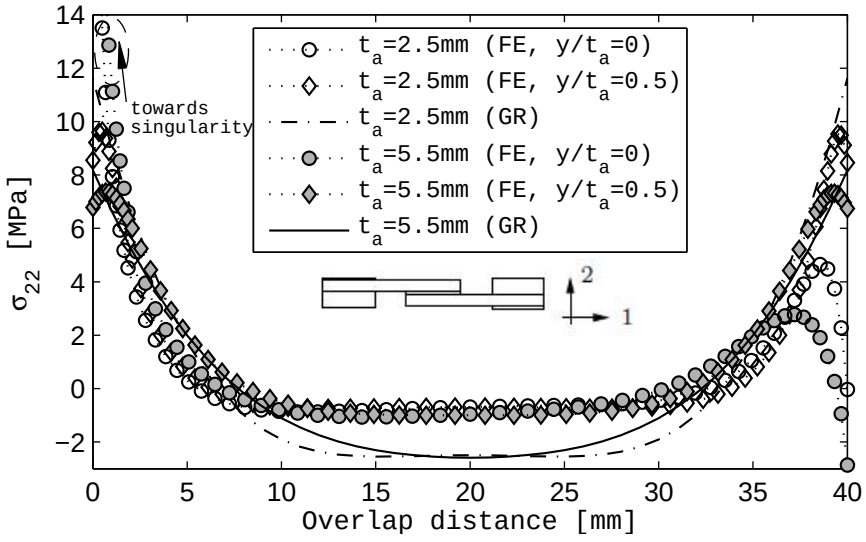

(a)

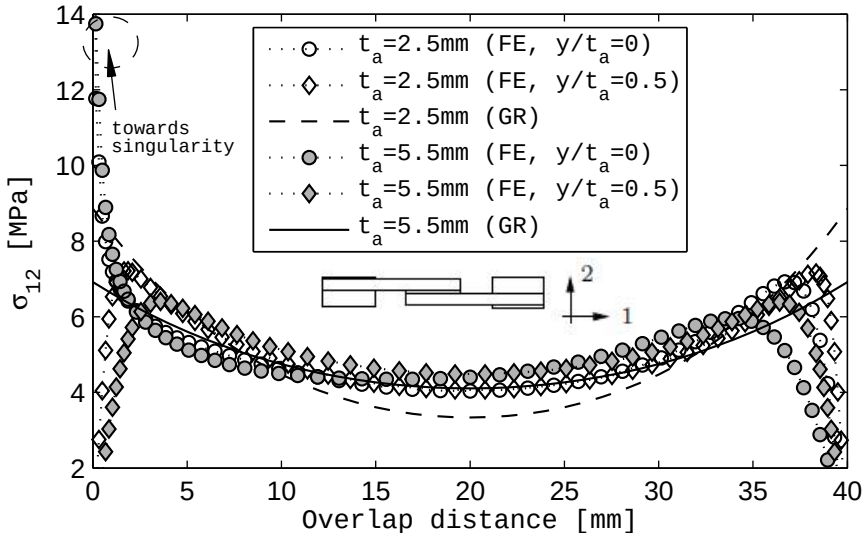

(b)

Figure 4: Comparison of (a) peel stress σ_{22} and (b) shear stress σ_{12} between prediction using finite element (FE) and Goland and Reissner (GR) theory, both at the interface and mid-section of adhesive bondline.

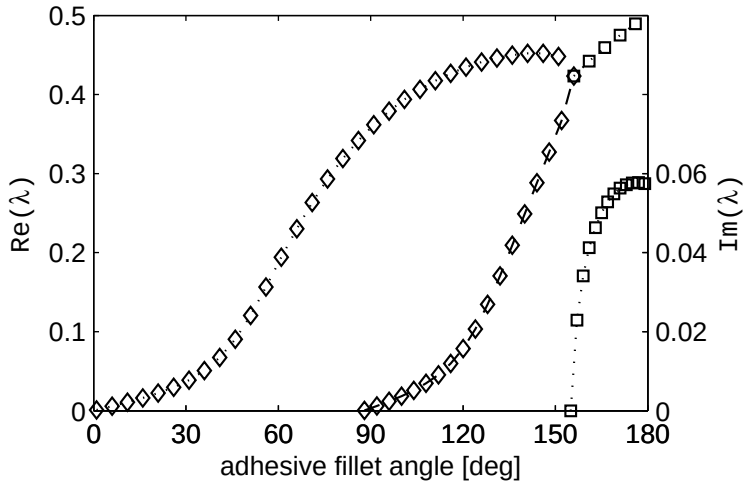

Figure 5: The analytical eigenvalues λ for isotropic-orthotropic bi-material corner.

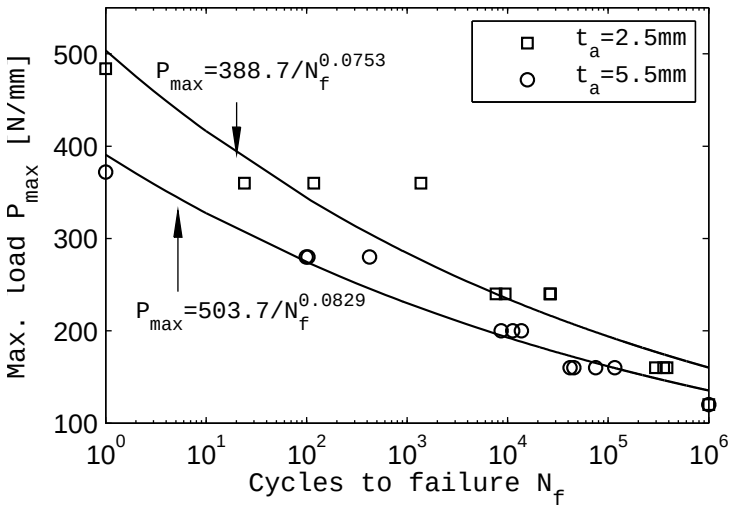

(a)

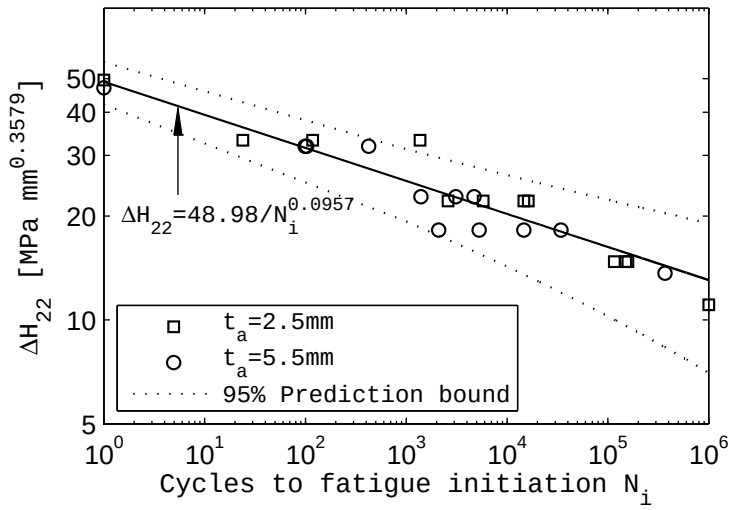

(b)

Figure 6: Effect of adhesive thickness on (a) total fatigue life and (b) fatigue initiation life of the bonded composite joints.

Table 1: Summary of quasi-static failure loads for SLJs and evaluation of critical generalized stress intensity factor.

Adhesive thickness t_a [mm]	Number of specimens	Average critical load P_{cr} [N/mm]	Ratio of final failure modes (M:I)[a]	$dH_{22}^{(1)}/dP_{FEM}$ [$\times 10^{-3}$ MPa·mm$^{1.3579}$/N]	H_{cr} [MPa·mm$^{0.3579}$]
2.5	6	484±62	4:2	102.40	49.56
5.5	6	372±50	6:0	126.50	47.06

[a]M, mixed interfacial-interlaminar mode; I, interfacial mode.

Table 2: A comparison of values of generalized stress intensity factors obtained within singularity zone of 0.0327 mm, at interface ($\theta = 0$).

Generalized stress intensity factors	$H_{ij}^{(1)}$ ($\lambda_1 = 0.3579$)	$H_{ij}^{(2)}$ ($\lambda_2 = 0.0032$)	Only $H_{ij}^{(1)}$ ($\lambda_1 = 0.3579$)
2.5 mm bondline thickness			
σ_{11}	14.27	-10.49	13.32
σ_{12}	8.41	-6.13	7.86
σ_{22}	20.48	-20.60	18.62
σ_{11} (adherend side)	69.17	35.68	72.39
5.5 mm bondline thickness			
σ_{11}	17.82	-15.91	16.55
σ_{12}	9.92	-5.03	9.52
σ_{22}	25.30	-26.60	23.18
σ_{11} (adherend side)	80.09	65.83	85.34

Table 3: Fatigue failure data for lap joints with adhesive thickness of (a) 2.5 mm (b) 5.5 mm.

(a)

Nominal maximum load P_{max} [N/mm]	Sample identification	Cycles to initiation N_i	Cycles to total failure N_f	Final failure mode[a]
360	9kN_ft01	1,368	1,368	M
	9kN_ft02	24	24	I
	9kN_ft03	118	118	M
240	6kN_ft01	14,700	26,284	M
	6kN_ft02	2,600	7,652	I
	6kN_ft03	16,200	26,732	M
	6kN_ft04	5,800	9,470	M
160	4kN_ft01	116,000	384,958	M
	4kN_ft02	150,000	356,126	M
	4kN_ft03	158,000	295,861	M
120	3kN_ft01	$> 10^6$	$> 10^6$	-
	3kN_ft02	$> 10^6$	$> 10^6$	-

[a]Final failure mode: M, mixed interfacial-interlaminar mode; I, interfacial mode.

(b)

Nominal maximum load P_{max} [N/mm]	Sample identification	Cycles to initiation N_i	Cycles to total failure N_f	Final failure mode[a]
280	7kN_ft01	423	423	M
	7kN_ft02	99	99	M
	7kN_ft03	103	103	I
200	5kN_ft01	4,700	11,240	M
	5kN_ft02	1,400	8,620	M
	5kN_ft03	3,100	13,731	M*
160	4kN_ft01	2,100	74,968	I*
	4kN_ft02	5,300	45,668	M*
	4kN_ft03	14,700	41,700	M*
	4kN_ft04	34,200	116,307	M*
120	3kN_ft01	369,200	$> 10^6$	-

[a]Final failure mode: M, mixed interfacial-interlaminar mode; I, interfacial mode. Superscript * indicates occurrence of propagation path at both adhesive-adherend interfaces.